UNIVERSITY OF LEEDS

This is a repository copy of *Assisted Magnetic Soft Continuum Robot Navigation via Rotating Magnetic Fields*.

White Rose Research Online URL for this paper:
https://eprints.whiterose.ac.uk/205180/

Version: Accepted Version

Article:
Chathuranga, D. orcid.org/0000-0001-6950-1848, Lloyd, P. orcid.org/0000-0002-4927-071X, Chandler, J.H. orcid.org/0000-0001-9232-4966 et al. (2 more authors) (2024) Assisted Magnetic Soft Continuum Robot Navigation via Rotating Magnetic Fields. IEEE Robotics and Automation Letters, 9 (1). pp. 182-190. ISSN 2377-3766

https://doi.org/10.1109/lra.2023.3331292

© 2023 IEEE. Personal use of this material is permitted. Permission from IEEE must be obtained for all other uses, in any current or future media, including reprinting/republishing this material for advertising or promotional purposes, creating new collective works, for resale or redistribution to servers or lists, or reuse of any copyrighted component of this work in other works.

Reuse
Items deposited in White Rose Research Online are protected by copyright, with all rights reserved unless indicated otherwise. They may be downloaded and/or printed for private study, or other acts as permitted by national copyright laws. The publisher or other rights holders may allow further reproduction and re-use of the full text version. This is indicated by the licence information on the White Rose Research Online record for the item.

Takedown
If you consider content in White Rose Research Online to be in breach of UK law, please notify us by emailing eprints@whiterose.ac.uk including the URL of the record and the reason for the withdrawal request.

White Rose university consortium
Universities of Leeds, Sheffield & York

eprints@whiterose.ac.uk
https://eprints.whiterose.ac.uk/

This article has been accepted for publication in IEEE Robotics and Automation Letters. This is the author's version which has not been fully edited and content may change prior to final publication. Citation information: DOI 10.1109/LRA.2023.3331292

Assisted Magnetic Soft Continuum Robot Navigation via Rotating Magnetic Fields

Damith Chathuranga[1], Peter Lloyd[1], James H. Chandler[1] *Member, IEEE*, Russell A. Harris[2] and Pietro Valdastri[1] *Fellow, IEEE*

***Abstract*—Innovative robotic catheters that are soft, flexible, and controlled by magnets have the potential to revolutionize minimally invasive surgical procedures in critical areas such as the lungs, brain and pancreas, which currently pose significant safe access challenges using existing technology. These shape forming millimetre-scale magnetic soft continuum robots (MSCRs) can be designed to be highly dexterous in order to access regions of the anatomy otherwise deemed inaccessible. However, due to their soft and slender nature, MSCRs are prone to buckling under compressive loads during insertion. In this study we demonstrate buckling free insertion of high aspect ratio (80 mm long by 2 mm diameter) MSCRs into narrow, tortuous lumens enabled by coupling a specific lengthwise magnetic profile with exposure to a rotating magnetic field (RMF). We present design, finite element modelling (FEM) of the motion, fabrication and actuation of three different MSCRs. These robots are cast from NdFeB doped silicone polymer to obtain 2 mm and 3 mm diameter catheters. These are magnetized in a predefined profile such that when the catheters are placed in an RMF, a serpentine motion is generated. Experiments were conducted to quantify the behaviour of these soft catheters navigating through a soft phantom that mimicked narrow tortuous lumens such as the pancreas and bile ducts. Oscillating actuation increased the inserted depth reached by the MSCR in a tortuous channel and even enabled squeezing through a 1 mm diameter opening via shape morphing. The experiments showed that an RMF reduced the required insertion forces by almost 45% and increased the distance inserted in a fixed time frame by 3 times.**

***Index Terms*—Surgical Robotics: Steerable Catheters/Needles; Soft Robot Applications; Medical Robots and Systems**

I. Introduction

OVER the last twenty years, medical robotics has experienced a surge in popularity and gained widespread acceptance among the medical community as delivering advanced and promising treatment approaches for conditions that traditionally required highly invasive surgical procedures. According to [1], continuum robots (CR) will continue to gain traction in surgery due to their significant advantage of high dexterity and ability to access and navigate small anatomical pathways. Beyond an increasing number of research platforms [2]–[4], CRs have made their way to patients via several commercial offerings including the Monarch (Auris Health, Inc. Redwood City, CA, USA), Galaxy (Noah medical, USA) and Ion (Intuitive Surgical, Inc. Sunnyvale, CA, USA).

CR structures may be manufactured from rigid components [5], soft components [6], [7], or a combination [8]. However, for CRs where the majority or entirety of its components are made from compliant polymeric materials, they may be classified as soft continuum robots (SCRs). Actuation of SCRs is possible by means of, for example, tendons [9]; fluidic (pneumatic and hydraulic) pressure [10]–[12]; shape memory alloys (SMA) [13]; or magnetic interaction [14], [15]. Of these actuation approaches, the use of magnetics offers the unique advantages of untethered actuation and miniaturization without loss of controllable degrees of freedom (DOF). These benefits give magnetic soft continuum robots (MSCRs) [16] the possibility to navigate through small, sensitive and tortuous pathways, and thus MSCR designs have been proposed as alternatives for traditional endoscopes and other forms of endoluminal devices [4]. In particular, miniature MSCRs have shown promise when it comes to navigating in soft and sensitive tissues at the millimetre scale, such as the peripheral lungs [17], pancreas [18], and vasculature [19]. MSCRs can be fabricated at low cost using a mix of base elastomer and magnetic micro-particles, giving them inherent structural softness to safely move inside small passages and achieve high curvatures along their entire length.

When considering motion through lumens, there are several examples of untethered microrobots designed to travel inside organs, veins and arteries propelled via an external magnetic field [20]–[23]. Tethered robots or catheters, such as commercially available steerable catheters (e.g. Polaris XTM Steerable Diagnostic Catheters by Boston Scientific Inc), magnetic steering guide wires [24], and concentric tubes [25], are introduced into the body by surgeons who mechanically push the catheter into the lumen. They then employ a combination of pushing, pulling, and twisting movements to manoeuvre the catheter to its intended destination. One significant limitation of these systems is their reliance on rigid structures to transmit the force applied by the surgeon to push the catheter into the

Manuscript received: July, 10, 2023; Revised October, 2, 2023; Accepted October, 27, 2023.

This paper was recommended for publication by Editor Jessica Burgner-Kahrs upon evaluation of the Associate Editor and Reviewers' comments

Research reported in this article was supported by the Royal Society, by the Engineering and Physical Sciences Research Council (EPSRC) under grant number EP/V009818/1. Any opinions, findings and conclusions, or recommendations expressed in this article are those of the authors and do not necessarily reflect the views of the Royal Society, or EPSRC.

For the purpose of open access, the authors have applied a Creative Commons Attribution (CCBY) license to any Accepted Manuscript version arising.

[1] Damith Chathuranga, Peter Lloyd, James H. Chandler, and Pietro Valdastri are with the STORM Lab, Institute of Autonomous Systems and Sensing (IRASS), School of Electronic and Electrical Engineering, University of Leeds, Leeds, UK.

[2] Russell A. Harris is with the School of Mechanical Engineering, University of Leeds, Leeds, UK. Email: {d.katudampevithanage, men9prl, j.h.chandler, R.harris p.valdastri}@leeds.ac.uk

Digital Object Identifier (DOI): see top of this page.

Authorized licensed use limited to: University of Leeds. Downloaded on November 10,2023 at 18:43:32 UTC from IEEE Xplore. Restrictions apply.
© 2023 IEEE. Personal use is permitted, but republication/redistribution requires IEEE permission. See https://www.ieee.org/publications/rights/index.html for more information.

This article has been accepted for publication in IEEE Robotics and Automation Letters. This is the author's version which has not been fully edited and content may change prior to final publication. Citation information: DOI 10.1109/LRA.2023.3331292

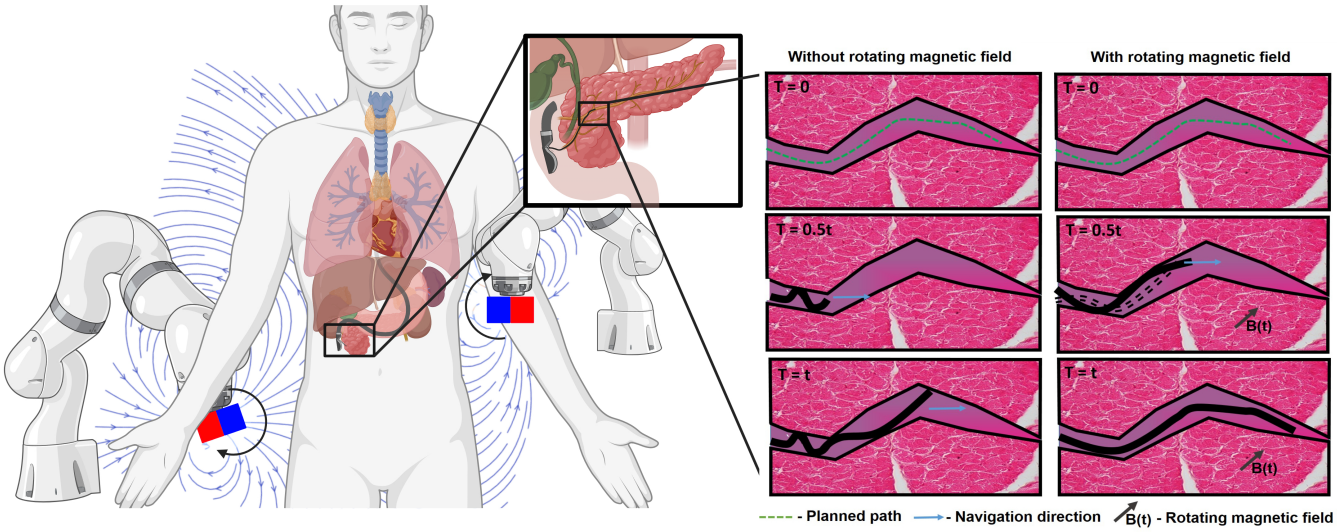

Fig. 1: The MSCR, deployed using a duodenoscope, is shown navigating within the pancreatic duct. The subfigures depict two scenarios: one illustrating the insertion of the MSCR into a section of the pancreatic duct without the use of a RMF, resulting in buckling, and the other demonstrating the insertion of the MSCR with the assistance of a RMF. The dashed lines represent the MSCR's serpentine-like motion. Illustrations were created using BioRender.com

lumen. These inherently stiff catheters have a propensity to cause tissue damage, such as acute pancreatitis, following surgery. Growing vine robots and similar tip extensions [26] are strategies for lumen navigation but have not yet achieved the millimetre scale of the proposed MSCR. Furthermore, there remains a gap in the literature relating to locomotion of tethered soft continuum robots and the challenges associated with navigation in soft narrow endoluminal pathways. These challenges are particularly apparent for miniaturized MSCRs, as reducing their cross sectional area causes an increase in aspect ratio, so that the MSCR, when pushed from its proximal end, has a proclivity to buckle under compressive stress. Similarly, pulling the MSCR from the distal end (e.g. via magnetic gradient pulling [27]), will not limit interactions between the robot's body and anatomical obstructions along the pathway; potentially limiting navigation progress and risking high axial strains and even snapping of the MSCR. Approaches delivering simultaneous proximal pushing with oscillatory reshaping of the MSCR's entire body may help mitigate buckling and avoid obstructions, thus improving the navigational ease for high aspect ratio MSCRs and allowing them to reach further along anatomical pathways.

In this paper, we introduce and evaluate an actuation strategy to aid high aspect ratio MSCRs to navigate safely through narrow and tortuous lumens. Initially, these robots are delivered to the surgical site via an endoscope (Fig.1). The approach combines two key elements: a rotating magnetic field (RMF) to dynamically reshape the robot and mechanical insertion from its distal end. This combination enables the robot to move in a 'snake-like' motion, allowing it to advance smoothly within compliant lumens of varying diameters without buckling or sticking. We examine the material composition of the MSCR (whether it's unreinforced or reinforced to limit specific undesired Degrees of Freedom), the MSCR's diameter, the lumen's diameter, and the RMF conditions required for successful lumen navigation.

II. Oscillating Magnetic Soft Continuum Robot

For the presented proof-of-concept, we consider the scenario of catheter insertion into the narrow delicate anatomy of the pancreatic duct. For effective surgical interventions involving the adult pancreas, this limits the diameter of the MSCR to between 2-3 mm [28]. A magnetically active length of 80 mm was selected for the body of the MSCR. As depicted in Fig. 1, the proposed design employs a time varying shape that mimics serpentine like wave motion during actuation to minimize contact between the MSCR and lumen walls as explained in [29]. Under the assumption of actuation being delivered via a time-varying, homogeneous applied magnetic field $B(t)$, this may be achieved using a continuously varying lengthwise magnetization profile $m(s)$, where s represents the position along the length of the MSCR ($s \in [0, L]$, where L is the length of the MSCR), with a sinusoidal profile. Rotation of the applied field will thus cause the shape profile of the MSCR to shift along its length in a repeating manner and in accordance with the relative frequency of the magnetization profile and applied field, inducing serpentine-like motion to assist navigation of the MSCR.

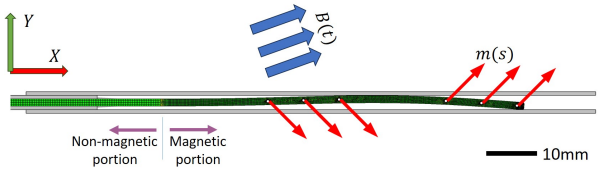

Fig. 2: 2 mm diameter MSCR represented using 5000 finite elements. Insertion is driven by an undamped prismatic joint, actuation induced by six discrete magnetic torques applied to six embedded 0.75 mm diameter rigid domains spaced at 10 mm centres. Torques calculated as functions of the magnetizations $m(s)$ (indicated here by red arrows) and a rotating applied field $B(t)$ (shown by blue arrows). Resistance to forward motion is a function of both gravity and the friction between the channel walls and the MSCR.

Authorized licensed use limited to: University of Leeds. Downloaded on November 10,2023 at 18:43:32 UTC from IEEE Xplore. Restrictions apply.
© 2023 IEEE. Personal use is permitted, but republication/redistribution requires IEEE permission. See https://www.ieee.org/publications/rights/index.html for more information.

This article has been accepted for publication in IEEE Robotics and Automation Letters. This is the author's version which has not been fully edited and content may change prior to final publication. Citation information: DOI 10.1109/LRA.2023.3331292

A. Modelling of MSCR

To verify our hypothesis, a quasi-static numerical simulation of the MSCR design under insertion into a silicone oil filled lumen was developed in Finite Element (FE) simulation software (COMSOL Multiphysics v5.6, COMSOL AB, Stockholm, Sweden) using the Multibody Dynamics module to simulate the mechanical response of the elastomer. To realize a computationally feasible solution of the complex physical system, a number of simplifying assumptions were made. Firstly, the simulation was built in two dimensions under the plane strain assumption ($\epsilon_z = 0$) as in [30]. The assumption of fully planar deformation (pure bending) is valid for MSCR that do not experience torsional strain [18] and as such we consider a plane strain model to be valid under this fully planar deformation. Secondly, to impart body torque in a stable manner, a mechanical moment was applied to a series of six, 0.75 mm diameter, rigid domains embedded along the length of the robot simulation, as shown in Fig. 2. As in [31], torques are calculated analytically, within each solver loop, as a function of applied field $B(t)$ and deformed magnetization $m(s)$ and encoded as a mechanical moment input. This eliminates the need for the electromagnetic module without material loss of accuracy. This approach circumvents the requirement to include direct consideration of simulated electromagnetic fields with their attendant non-linearity.

To most reliably adhere to the torsion-free requirements of the plane strain condition, the MSCR was modelled with a 2 mm diameter and a 1 mm axially aligned braid reinforcement. The magnitude of the magnetization vector of each of the six segments along the length was thus simulated as a 2 mm outer diameter, 1 mm inner diameter magnetic silicone segment with a length of 10 mm and a 50% by weight concentration of NdFeB particles. This results in a remnant magnetization of 0.11 mT [32] and a modulus of elasticity, which considers the mechanical effects of the braid, of 500 kPa [18]. The orientations of the magnetization vectors are shown in Fig. 2 and actuated subject to a rotating magnetic B field of peak magnitude 28 mT.

To capture the insertion force, the base of the tentacle was attached to an undamped prismatic joint with an applied push force set as a simulation variable. This tentacle-joint arrangement was advanced as a function of time into a 4 mm diameter channel made of rigid encastred, straight walls with a Coulomb friction coefficient between the lubricated wall and tentacle of 0.07 [33]. For all models an effective density of $200kg/m^3$ was calculated considering the buoyancy of the tentacle in silicone oil. In the magnetically actuated simulation, friction exists at discrete upper and lower points of contact as the tentacle shape forms along it's own length. For the unactuated simulation, friction occurs exclusively and continuously along the bottom of the channel where contact occurs due to gravity.

All models were meshed using quadrilateral elements free formed via the COMSOL auto-mesh generator. This produced 5000 finite elements and took, on average, 192 seconds to converge utilizing Newton-Raphson iterations within the MUltifrontal Massively Parallel sparse direct Solver (MUMPS) option. For a 20 time step transient simulation, this represents a 64 minute mean run-time on a 3.2 GHz, 32 GB, 16 core Intel Xeon Gold processor. Simulations were performed with either fixed insertion velocity of 1 mm/s or fixed insertion force of 0.2 N and with and without an external rotating B field of 28 mT at 3 Hz.

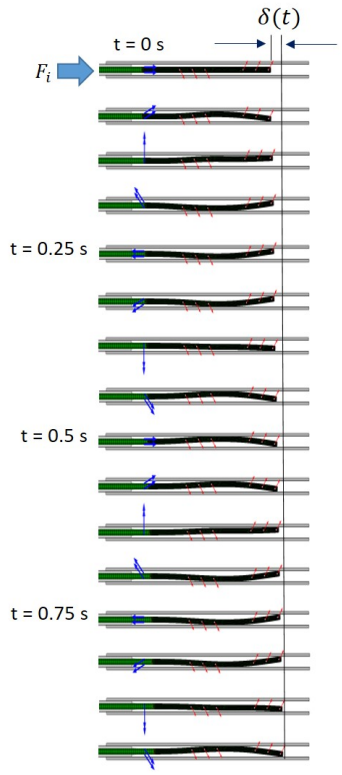

Fig. 3: FEA simulated data demonstrating the MSCR's serpentine motion in a straight lumen, driven by a RMF of 2Hz. Insertion force (F_i) is calculated when the MSCR is inserted at a speed of 1 mm/s ($\delta(t) = 1mm$). Dark blue arrows indicate the RMF direction with time, while red arrows show MSCR segment magnetization.

B. Numerical Results

Simulation results for a fixed insertion velocity of 1 mm/s showed a peak insertion force F_i (see Fig.3) at the base of the tentacle of 0.17 N under a 3 Hz rotating B field of 28 mT and 0.19 N under no rotating field ($B(t)$ = 0 mT). This translates as an 11% reduction in required insertion force as a consequence of the application of the rotating B field. For simulations with a constant insertion force of 0.2 N, applied for 50 seconds, final insertion depths were measured as 268 mm and 180 mm for insertions with and without a 28 mT, 3 Hz rotating B field respectively. Application of the rotating applied field in this case therefore showed an increased penetration depth of 49%. Furthermore, the simulation demonstrated the MSCR navigating in the lumen in a serpentine like motion as seen in Fig.3.

III. Experimental Verification

To evaluate the proposed MSCR navigation approach of utilising an RMF to assist motion through a narrow passage without buckling under the insertion force, two experiments

Authorized licensed use limited to: University of Leeds. Downloaded on November 10,2023 at 18:43:32 UTC from IEEE Xplore. Restrictions apply.
© 2023 IEEE. Personal use is permitted, but republication/redistribution requires IEEE permission. See https://www.ieee.org/publications/rights/index.html for more information.

This article has been accepted for publication in IEEE Robotics and Automation Letters. This is the author's version which has not been fully edited and content may change prior to final publication. Citation information: DOI 10.1109/LRA.2023.3331292

TABLE I: MSCR specifications

Identification	External diameter(mm)	Material	Reinforced (yes/no)
MSCR i	2	Ecoflex 30 and NdFeB particles (1:1 ratio)	no
MSCR ii	2	Ecoflex 30 and NdFeB particles (1:1 ratio)	yes (1mm Nylon braid)
MSCR iii	3	Ecoflex 30 and NdFeB particles (1:1 ratio)	no

were performed. The first was designed following the conditions of the FE simulation to measure the insertion force of the MSCR with and without application of an RMF. The second experiment targeted identification of optimal parameters and the assessment of the ability of the MSCR to move through a tortuous narrowing lumen, more representative of our target clinical application.

A. Fabrication of MSCRs

For the experimental testing, three MSCR designs were fabricated with the design parameters shown in Table I. Fully soft MSCR designs were fabricated with a constant diameter of 2 mm and 3 mm respectively, and with an active magnetic length of 80 mm. To observe the influence of increased axial stiffness, an additional 2 mm diameter MSCR was fabricated to include a braided reinforcement.

The fabrication process is outlined in Fig. 4. The 2 mm designs were cast inside a 2 mm internal diameter perspex tube. For the braided MSCR, a nylon braid of external diameter 1 mm (Everlasto - James Lever 1856 Ltd, Manchester, U.K.) was inserted into the tube and held in axial alignment using 3D printed end-caps (Fig.4(a)). Properties of this braided MSCR are stated in [18]. For the 3 mm diameter MSCR, the mould cavity was 3D printed (PLA, UltiMaker S5, UltiMaker, Netherlands), as shown in Fig.4(b). Each tube/mould was filled with a mixture of Ecoflex-0030 (Smooth-On Inc, USA) and neodymium-iron-boron (NdFeB) microparticles with an average diameter of 5 μm (MQFP-B+, Magnequench GmbH, Germany) in a mass ratio of 1:1. This composite was mixed and degassed in a high vacuum mixer (ARV-310, THINKYMIXER, Japan) at 1400 rpm, 20.0 kPa for 90 seconds, and injected into the tubing/moulds and cured at room temperature for four hours. Specimens are shown in Fig.4(c). Upon removal from the mould, the specimens were secured into a 3D printed magnetizing tray (Fig.4(d)) before being magnetized using an impulse magnetic field of 4.644 T (ASC IM-10-30, ASC Scientific, USA). The half sinusoidal shape of the magnetization tray was decided such that it would produce the largest deformation possible when a perpendicular field was applied to the MSCR. The amplitude and wavelength of the sinusoidal wave was dictated by the physical limitations of the magnetization coil dimensions.

B. Insertion force evaluation

To evaluate just the insertion force eliminating side wall interactions at bends, the MSCR designs were pushed into soft lumen phantoms (straight lumen with diameters of 4 mm, 5 mm or 6 mm in the horizontal plane) using a linear actuator (igus MOT-AN-S-060-005-042-L-A-AAA), as shown in Fig.5. Care was taken to keep the MSCR plane of actuation parallel to the magnetization tray plane. This was achieved by marking the MSCR's vertical plane and keeping it perpendicular to the xy plane in Fig.5. The tentacle was connected to the linear actuator through a force/torque sensor (Nano 17, ATI corporation) such that the insertion force was recorded by the force sensor in the x direction. Other force directions were disregarded as F_x is the significant indicator for the experiment. Two permanent N42 Neodymium magnets of the size 50 mm×50 mm×25 mm (Bunting Inc.) were each fixed on top of a servo actuator (My Actuator RMD-X8 1:9) using 3D printed mounts. The actuators were programmed using a Controller Area Network protocol (CAN bus) using a microchip CAN analyser to allow synchronous rotation up to a maximum of 170 rpm. The rotating magnets generate a magnetic field that changes the direction relative to the orientation of the magnets. These magnets generate an uniform field that flips its direction every half revolution [34] (see Fig.6, which displays the magnetic field lines simulated by using the Magpylib 4.2.0 package in Python). Thus, the rotating field of the magnet is proportional to the angular velocity with which the two magnets rotate. For this experiment the magnets were rotated with angular velocities equivalent to 120 and 170 rpm (rotating frequency of 2, and ∼3 Hz respectively), generating a peak magnetic field strength of 28 mT, as measured using a magnetic field sensor (F71 Multi-axis teslameter, Lake Shore Cryotronics Inc.) (see Fig.7(c) of time varying magnetic field strength values of a point in the green dashed line). The servo actuators were fixed to a second linear actuator (Thorlabs NRT150/M) that could be moved along the long (x) axis of the phantom. This was so that the MSCR was always in the working area of the rotating magnets as it traveled along the lumen.

Soft phantoms representing the narrow passageways of the human anatomy were fabricated and suspended symmetrically between the two axes of the actuating magnets. Phantoms were fabricated from silicone gel (EcoFlex Gel 2, Smooth-On, Inc, USA) to represent the soft structure of the pancreas with either a 4, 5, or 6 mm diameter lumen. Each lumen was subsequently filled with PDMS silicone oil of viscosity 20 cSt (Aldrich Inc.) to lubricate and mimic the aqueous nature of internal anatomy.

Insertion force tests were performed by inserting the MSCR at a speed of 0.25 mm/s into the phantom while recording the time stamped force $f_x(t)$. The force $f_x(t)$ was measured while the MSCR of length 80 mm was completely inserted and pushed an additional 10 mm into the lumen. For each tentacle design and lumen diameter combination, the insertion was repeated five times under each conditions of: 0 Hz (no rotating field), 2 Hz and 3 Hz. The average maximum insertion force F_x was calculated for each lumen size and rotating field combination by determining the average (mean) maximum insertion force across all tentacle designs and repeats.

C. Phantom lumen experiments

Fig. 7(a) shows the setup of the second set of experiments: phantom lumen trials. The phantom was cast in such a way

Authorized licensed use limited to: University of Leeds. Downloaded on November 10,2023 at 18:43:32 UTC from IEEE Xplore. Restrictions apply.
© 2023 IEEE. Personal use is permitted, but republication/redistribution requires IEEE permission. See https://www.ieee.org/publications/rights/index.html for more information.

This article has been accepted for publication in IEEE Robotics and Automation Letters. This is the author's version which has not been fully edited and content may change prior to final publication. Citation information: DOI 10.1109/LRA.2023.3331292

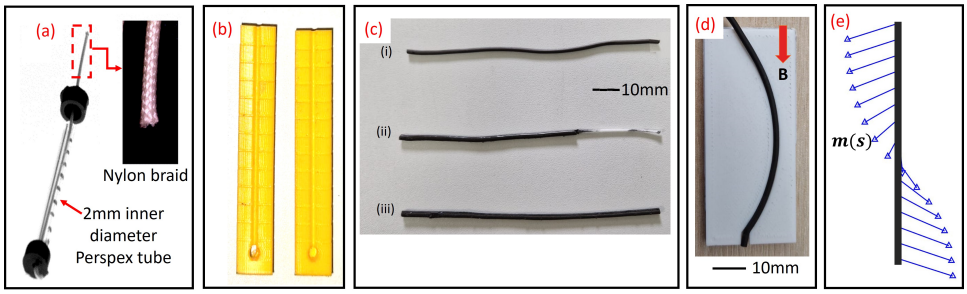

Fig. 4: Steps of MSCR fabrication. (a) Fabrication of the braided MSCR (ii) by inserting a 1 mm diameter nylon braid into the perspex tube before injecting doped elastomer. (b) Moulds used for the 3 mm MSCR cast. (c) Fabricated MSCR - (i) 2 mm diameter (ii) 2 mm diameter reinforced (iii) 3 mm diameter MSCR. (d) The MSCR was magnetized using an impulse magnetic field of direction shown in the red arrow by inserting it in a tray to hold the shape (e) magnetization $m(s)$ along the MSCR

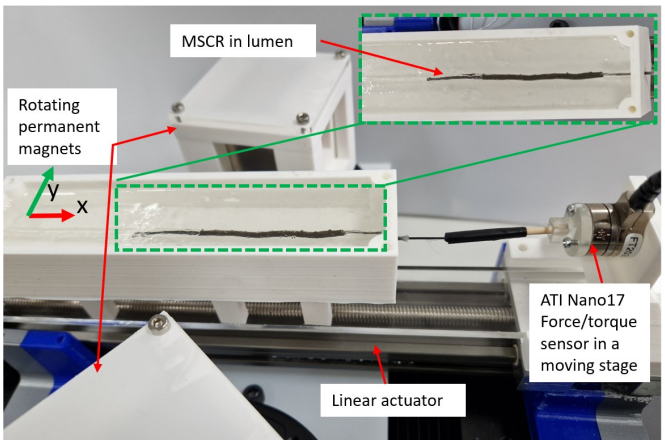

Fig. 5: Insertion force experimental setup: The MSCR was fixed to a linear stage via ATI Nano 17 force/torque sensor. MSCR was inserted into the endoluminal phantom using the linear actuator. The synchronously rotating permanent magnets on the either side of the phantom produced the RMF.

that the cavity was tortuous and the channel diameter started at 3 mm, reducing to 1 mm at the third bend. This represents an idealized anatomical scenario with similarity to the pancreatic duct geometry from [35]. Insertion was carried out manually to simulate catheter insertion in realistic operating room conditions with visual feedback.

Three configurations were evaluated, firstly, a ground truth experiment with no RMF. In this scenario, the servo actuators were disabled and moved to the farthest end of the phantom. The MSCRs were inserted manually and video was recorded for a time of 50 seconds. The CR was pushed into the channel and rotated while inserted to move along the channel. Five trials were completed for each MSCR and the maximum length the MSCR reached was recorded.

For the next set of experiments, the servo actuators were turned on and rotated at a speed of 120 rpm. Together with the rotation, the two actuators were moved from the proximal end of the phantom to the distal end in a speed of 2 mm/s by the Thorlabs linear actuator. While this motion is in play, the MSCR was inserted into the channel similarly to earlier. The experiment ran for 50 seconds and five trials each for the three types of MSCR were performed. The maximum length the MSCR traveled was again recorded.

IV. Results

The average (mean$\pm$ max and min) recorded maximum insertion forces for each lumen diameter against the magnetic field rotation frequency are presented Fig. 8. The three colours represent the three diameters of the phantom lumen and the average x directional force measured by the force sensor. The average of 5 trials of each MSCR types combined is plotted with the maximum and minimum values for each frequency.

Fig. 9 and 10 pertain to the second set of experiments where the length of the insertion of the three types of MSCR was recorded over a 50 second period in the presence/absence of a RMF. Fig. 9 shows the insertion progression through the lumen at different time intervals for the three types of MSCR, with the average (mean $\pm$ max and min) final insertion distances measured reported in Fig. 10. From Fig. 9, it is evident that application of the RMF increases the achievable insertion depth for all MSCR designs; with the quantitative difference reached across repeat trials for each (Fig. 10) being statistically significant. For the different MSCR designs, a similar insertion distance for the 2 mm designs was shown (104.8 mm vs 105.8 mm for type i vs type ii, respectively), while the 3 mm diameter (type iii) design was only able to achieve an insertion distance of 66.5 mm.

V. Discussion and Future Work

The first experiment was conducted to measure the force required to insert the MSCR into a lumen in the absence/presence of an RMF. Fig. 8 demonstrates higher insertion forces of between 0.22 - 0.26 N for all three lumen sizes and MSCR types when no magnetic field was applied to the MSCR vs 0.10 - 0.15 N for tests with an RMF. This reduction (45% on average) is as a result of the presence of time-varying magnetic body torques on the MSCR. As the insertion force F_x can be interpreted as the counter-balance of friction forces between common contact areas of the lumen wall and the MSCR, it is apparent that the introduction of magnetically induced serpentine-like motion reduces and changes surface contact between MSCR and the lumen, reducing in turn the resultant frictional force resisting insertion. This aligns with observations of serpentine motion, where only a portion of the snake's body is touching the ground when in locomotion, [29]. Even though fluid filled anatomical scenarios may result in low friction values, for fully soft MSCRs it is critical to minimise

Authorized licensed use limited to: University of Leeds. Downloaded on November 10,2023 at 18:43:32 UTC from IEEE Xplore. Restrictions apply.
© 2023 IEEE. Personal use is permitted, but republication/redistribution requires IEEE permission. See https://www.ieee.org/publications/rights/index.html for more information.

This article has been accepted for publication in IEEE Robotics and Automation Letters. This is the author's version which has not been fully edited and content may change prior to final publication. Citation information: DOI 10.1109/LRA.2023.3331292

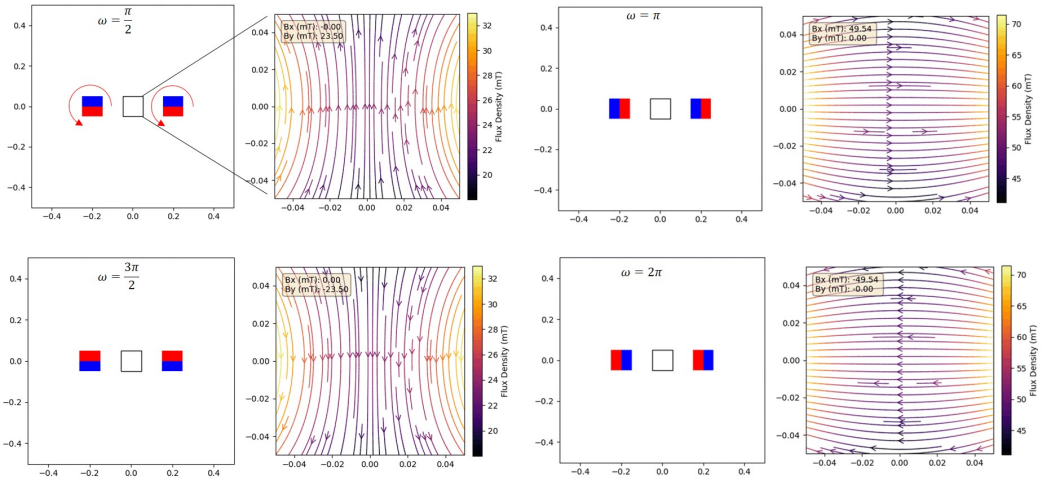

Fig. 6: Representation of the RMF generated at a square work envelope in the middle of the plot when permanent magnets represented in red and blue are rotating with zero phase shift

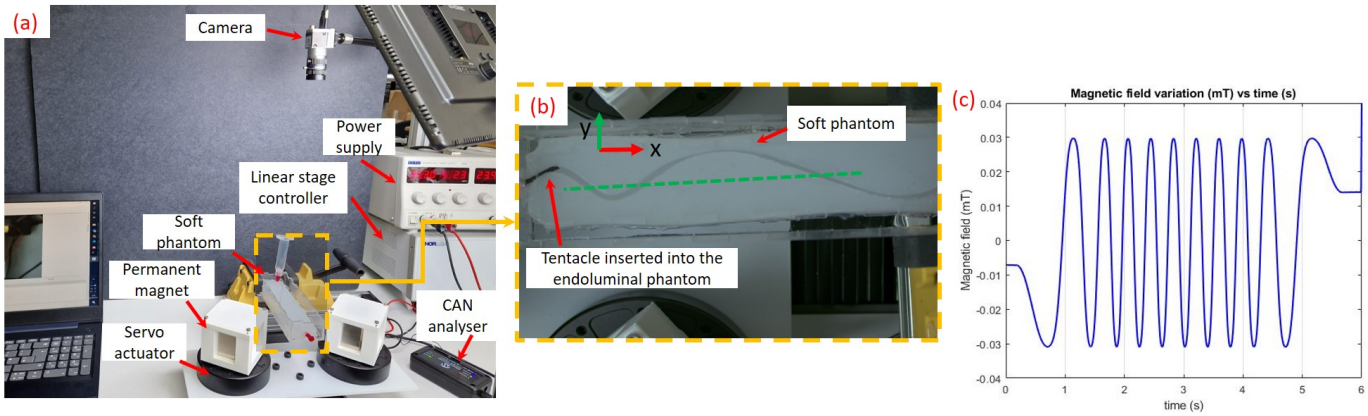

Fig. 7: (a) Phantom lumen trials setup. (b) Soft phantom was placed between two permanent magnets that rotate synchronously under servo actuator control. (c)Time varying magnetic field strength values on a point in the green line represented in (b) when the magnets rotate.

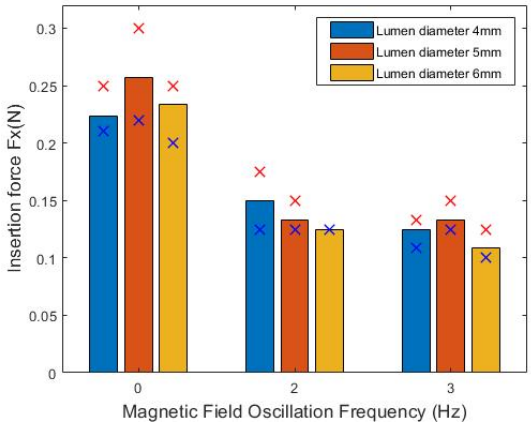

Fig. 8: Variation of the insertion force under the RMF taken as an average for all three types of MSCR. Red markers represent the maximum value obtained for each trial while blue marker represents the minimum value.

this value to avoid buckling during insertion from the proximal end and to thus assist forward motion. Although the RMF greatly reduces the measured insertion force, the presented findings from FEA simulations show little influence from its specific frequency, suggesting that this parameter may be varied to suit the practical constraints of a specific application. Actual experiments could not be conducted beyond 3 Hz due to experimental setup limitations.

The potential impact of RMF assistance was demonstrated via insertions into a soft, tortuous, narrowing lumen phantom, Fig. 9. Through application of a dynamic magnetic field, the MSCRs were able to be inserted 300% further than with no field (Fig. 10). Additionally, rotating field assistance allowed the 2 mm diameter MSCRs to be inserted between 4 and 7mm into the 1 mm diameter section of the soft lumen, indicating that this approach may allow fully soft MSCRs to pass through obstacles restricting the width of the endoluminal passage to below their nominal diameter. It is noted, however, that this characteristic is a function of the stiffness of the MSCR and of the phantom, and thus requires future investigation beyond the scope of this publication. Furthermore, while MSCR i and ii exhibited the same insertion length performance, MSCR ii, with its braided reinforcement, emerges as the preferred choice for practical applications. This is driven by its axial stiffness, which resist wrench, and its capability to accommodate tools such as optical fibres and flexible needles within its cavity.

There is a discrepancy between the experimental and numerical results as a consequence of some of the assumptions specified in order to make the simulation tractable. In particular, the wall boundary conditions specified in Section II-A (a straight

Authorized licensed use limited to: University of Leeds. Downloaded on November 10,2023 at 18:43:32 UTC from IEEE Xplore. Restrictions apply.
© 2023 IEEE. Personal use is permitted, but republication/redistribution requires IEEE permission. See https://www.ieee.org/publications/rights/index.html for more information.

This article has been accepted for publication in IEEE Robotics and Automation Letters. This is the author's version which has not been fully edited and content may change prior to final publication. Citation information: DOI 10.1109/LRA.2023.3331292

Fig. 9: Movement of the three types of MSCR with or without an RMF within a 50s time interval.

and rigid channel as opposed to curvilinear and materially soft) introduce significant error. As such, numerical results are considered to be physically representative as opposed to numerically accurate: These simulation results confirm that the application of an rotating B field reduces the required push force (Trial 1) and increases the achievable depth (Trial 2), but give no meaningful quantification of this phenomena. Given the complexity of material interactions involved in the physical experiments, a more sophisticated numerical simulation with quantitatively accurate output would be a challenging but desirable future work. Such a model would also allow insight into the localized strains and resultant changes in stiffness of the tentacle during navigation, potentially enabling future design optimization.

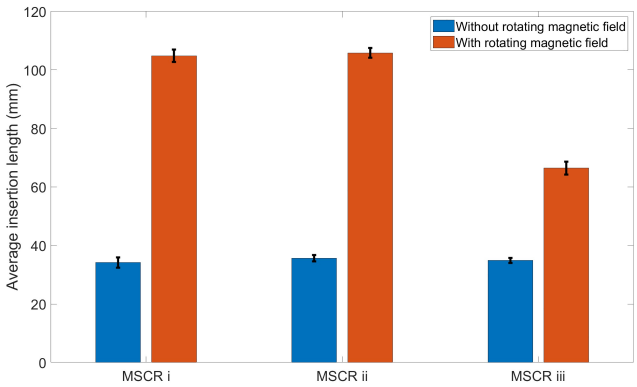

Fig. 10: Average insertion length after 50 seconds with respect to the presence/absence of RMF.

The presented method of driving a MSCR with sinusoidal magnetization via an rotating magnetic field has been shown to significantly reduce the required insertion force into a compliant lumen (∼45%) and assisted MSCRs in increasing the insertion reach over a fixed time period by more than a factor of three. This enabling approach has the potential to expand the scope of ultra low material stiffness high aspect ratio magnetic catheters, allowing for safer devices with improved anatomical access within endoluminal surgeries and potentially automate the catheter insertion process by impedance control [36].

This proposed method could be combined with an imaging technique like fluoroscopy to facilitate planning a path for the magnet's movement within the operating room. By providing the RMF via the rotating magnets of a dual robotic manipulation system such as [27], this could maintain perpendicular alignment to the path enabling both navigation and bifurcation

Authorized licensed use limited to: University of Leeds. Downloaded on November 10,2023 at 18:43:32 UTC from IEEE Xplore. Restrictions apply.
© 2023 IEEE. Personal use is permitted, but republication/redistribution requires IEEE permission. See https://www.ieee.org/publications/rights/index.html for more information.

This article has been accepted for publication in IEEE Robotics and Automation Letters. This is the author's version which has not been fully edited and content may change prior to final publication. Citation information: DOI 10.1109/LRA.2023.3331292

control at the same time. Exploring this possibility further presents an exciting avenue for future research.

VI. Acknowledgement

The authors thank Samwise Wilson and Robyn Finn for their technical assistance, Joshua Davy for the visual representation of the RMF, and BioRender.com.

References

[1] P. E. Dupont, B. J. Nelson, M. Goldfarb, B. Hannaford, A. Menciassi, M. K. O'Malley, N. Simaan, P. Valdastri, and G.-Z. Yang, "A decade retrospective of medical robotics research from 2010 to 2020," *Science Robotics*, vol. 6, no. 60, p. eabi8017, 2021.

[2] P. E. Dupont, N. Simaan, H. Choset, and C. Rucker, "Continuum robots for medical interventions," *Proceedings of the IEEE*, vol. 110, no. 7, pp. 847–870, 2022.

[3] J. Burgner-Kahrs, D. C. Rucker, and H. Choset, "Continuum robots for medical applications: A survey," *IEEE Transactions on Robotics*, vol. 31, no. 6, pp. 1261–1280, 2015.

[4] T. da Veiga, J. H. Chandler, P. Lloyd, G. Pittiglio, N. J. Wilkinson, A. K. Hoshiar, R. A. Harris, and P. Valdastri, "Challenges of continuum robots in clinical context: a review," *Progress in Biomedical Engineering*, vol. 2, no. 3, p. 032003, 2020.

[5] J. Peirs, D. Reynaerts, H. Van Brussel, G. De Gersem, and H.-W. Tang, "Design of an advanced tool guiding system for robotic surgery," in *2003 IEEE International Conference on Robotics and Automation (Cat. No.03CH37422)*, vol. 2, 2003, pp. 2651–2656 vol.2.

[6] A. D. Marchese and D. Rus, "Design, kinematics, and control of a soft spatial fluidic elastomer manipulator," *The International Journal of Robotics Research*, vol. 35, no. 7, pp. 840–869, 2016.

[7] M. Cianchetti, T. Ranzani, G. Gerboni, T. Nanayakkara, K. Althoefer, P. Dasgupta, and A. Menciassi, "Soft robotics technologies to address shortcomings in today's minimally invasive surgery: The stiff-flop approach," *Soft Robotics*, vol. 1, no. 2, pp. 122–131, 2014.

[8] B. L. Conrad and M. R. Zinn, "Interleaved continuum-rigid manipulation: An approach to increase the capability of minimally invasive surgical systems," *IEEE/ASME Transactions on Mechatronics*, vol. 22, no. 1, pp. 29–40, 2017.

[9] T. Zhang, L. Yang, X. Yang, R. Tan, H. Lu, and Y. Shen, "Millimeter-scale soft continuum robots for large-angle and high-precision manipulation by hybrid actuation," *Advanced Intelligent Systems*, vol. 3, no. 2, p. 2000189, 2021.

[10] J. D. Greer, T. K. Morimoto, A. M. Okamura, and E. W. Hawkes, "A soft, steerable continuum robot that grows via tip extension," *Soft robotics*, vol. 6, no. 1, pp. 95–108, 2019.

[11] M. A. Robertson, O. C. Kara, and J. Paik, "Soft pneumatic actuator-driven origami-inspired modular robotic "pneumagami"," *The International Journal of Robotics Research*, vol. 40, no. 1, pp. 72–85, 2021.

[12] Q. Xie, T. Wang, S. Yao, Z. Zhu, N. Tan, and S. Zhu, "Design and modeling of a hydraulic soft actuator with three degrees of freedom," *Smart Materials and Structures*, vol. 29, no. 12, p. 125017, 2020.

[13] J.-E. Shim, Y.-J. Quan, W. Wang, H. Rodrigue, S.-H. Song, and S.-H. Ahn, "A smart soft actuator using a single shape memory alloy for twisting actuation," *Smart Materials and Structures*, vol. 24, no. 12, p. 125033, 2015.

[14] S. Jeon, A. K. Hoshiar, K. Kim, S. Lee, E. Kim, S. Lee, J.-y. Kim, B. J. Nelson, H.-J. Cha, B.-J. Yi *et al.*, "A magnetically controlled soft microrobot steering a guidewire in a three-dimensional phantom vascular network," *Soft robotics*, vol. 6, no. 1, pp. 54–68, 2019.

[15] D. Liu, X. Liu, Z. Chen, Z. Zuo, X. Tang, Q. Huang, and T. Arai, "Magnetically driven soft continuum microrobot for intravascular operations in microscale," *Cyborg and Bionic Systems*, vol. 2022, 2022.

[16] L. Wang, C. F. Guo, and X. Zhao, "Magnetic soft continuum robots with contact forces," *Extreme Mechanics Letters*, vol. 51, p. 101604, 2022.

[17] G. Pittiglio, P. Lloyd, T. da Veiga, O. Onaizah, C. Pompili, J. H. Chandler, and P. Valdastri, "Patient-specific magnetic catheters for atraumatic autonomous endoscopy," *Soft Robotics*, vol. 9, no. 6, pp. 1120–1133, 2022.

[18] P. Lloyd, O. Onaizah, G. Pittiglio, D. K. Vithanage, J. H. Chandler, and P. Valdastri, "Magnetic soft continuum robots with braided reinforcement," *IEEE Robotics and Automation Letters*, vol. 7, no. 4, pp. 9770–9777, 2022.

[19] Y. Kim, E. Genevriere, P. Harker, J. Choe, M. Balicki, R. W. Regenhardt, J. E. Vranic, A. A. Dmytriw, A. B. Patel, and X. Zhao, "Telerobotic neurovascular interventions with magnetic manipulation," *Science Robotics*, vol. 7, no. 65, p. eabg9907, 2022.

[20] M. Richter, M. Kaya, J. Sikorski, L. Abelmann, V. Kalpathy Venkiteswaran, and S. Misra, "Magnetic soft helical manipulators with local dipole interactions for flexibility and forces," *Soft Robotics*, 2023.

[21] J. A. Steiner, L. N. Pham, J. J. Abbott, and K. K. Leang, "Modeling and analysis of a soft endoluminal inchworm robot propelled by a rotating magnetic dipole field," *Journal of Mechanisms and Robotics*, vol. 14, no. 5, p. 051002, 2022.

[22] L. N. Pham, J. A. Steiner, K. K. Leang, and J. J. Abbott, "Soft endoluminal robots propelled by rotating magnetic dipole fields," *IEEE Transactions on Medical Robotics and Bionics*, vol. 2, no. 4, pp. 598–607, 2020.

[23] A. Bhattacharjee, L. W. Rogowski, X. Zhang, and M. J. Kim, "Untethered soft millirobot with magnetic actuation," in *2020 IEEE International Conference on Robotics and Automation (ICRA)*. IEEE, 2020, pp. 3792–3798.

[24] S. Jeon, A. K. Hoshiar, K. Kim, S. Lee, E. Kim, S. Lee, J.-y. Kim, B. J. Nelson, H.-J. Cha, B.-J. Yi, and H. Choi, "A magnetically controlled soft microrobot steering a guidewire in a three-dimensional phantom vascular network," *Soft Robotics*, vol. 6, no. 1, pp. 54–68, 2019.

[25] P. E. Dupont, J. Lock, B. Itkowitz, and E. Butler, "Design and control of concentric-tube robots," *IEEE Transactions on Robotics*, vol. 26, no. 2, pp. 209–225, 2010.

[26] M. Li, R. Obregon, J. J. Heit, A. Norbash, E. W. Hawkes, and T. K. Morimoto, "Vine catheter for endovascular surgery," *IEEE Transactions on Medical Robotics and Bionics*, vol. 3, no. 2, pp. 384–391, 2021.

[27] G. Pittiglio, J. H. Chandler, M. Richter, V. K. Venkiteswaran, S. Misra, and P. Valdastri, "Dual-arm control for enhanced magnetic manipulation," in *2020 IEEE/RSJ International Conference on Intelligent Robots and Systems (IROS)*. IEEE, 2020, pp. 7211–7218.

[28] D. Teilum, "In vitro measurement of the length of the sphincter of oddi," *Endoscopy*, vol. 23, no. 03, pp. 114–116, 1991.

[29] S. Ma, H. Araya, and L. Li, "Development of a creeping snake-robot," in *Proceedings 2001 IEEE International Symposium on Computational Intelligence in Robotics and Automation (Cat. No. 01EX515)*. IEEE, 2001, pp. 77–82.

[30] P. Lloyd, A. K. Hoshiar, T. da Veiga, A. Attanasio, N. Marahrens, J. H. Chandler, and P. Valdastri, "A learnt approach for the design of magnetically actuated shape forming soft tentacle robots," *IEEE Robotics and Automation Letters*, vol. 5, no. 3, pp. 3937–3944, 2020.

[31] P. Lloyd, Z. Koszowska, M. Di Lecce, O. Onaizah, J. H. Chandler, and P. Valdastri, "Feasibility of fiber reinforcement within magnetically actuated soft continuum robots," *Frontiers in Robotics and AI*, vol. 8, p. 715662, 2021.

[32] T. Da Veiga, J. H. Chandler, G. Pittiglio, P. Lloyd, M. Holdar, O. Onaizah, A. Alazmani, and P. Valdastri, "Material characterization for magnetic soft robots," in *2021 IEEE 4th International Conference on Soft Robotics (RoboSoft)*, 2021, pp. 335–342.

[33] C. Rotella, B. Persson, M. Scaraggi, and P. Mangiagalli, "Lubricated sliding friction: Role of interfacial fluid slip and surface roughness," *The European Physical Journal E*, vol. 43, no. 2, p. 9, 2020.

[34] W. Zhang, Y. Meng, and P. Huang, "A novel method of arraying permanent magnets circumferentially to generate a rotation magnetic field," *IEEE trans. on magnetics*, vol. 44, no. 10, pp. 2367–2372, 2008.

[35] M. Sugimoto, S. Takahashi, M. Kojima, N. Gotohda, Y. Kato, S. Kawano, A. Ochiai, and M. Konishi, "What is the nature of pancreatic consistency? assessment of the elastic modulus of the pancreas and comparison with tactile sensation, histology, and occurrence of postoperative pancreatic fistula after pancreaticoduodenectomy," *Surgery*, vol. 156, no. 5, pp. 1204–1211, 2014.

[36] J. Jayender, R. Patel, and S. Nikumb, "Robot-assisted active catheter insertion: Algorithms and experiments," *The International Journal of Robotics Research*, vol. 28, no. 9, pp. 1101–1117, 2009.

Authorized licensed use limited to: University of Leeds. Downloaded on November 10,2023 at 18:43:32 UTC from IEEE Xplore. Restrictions apply.
© 2023 IEEE. Personal use is permitted, but republication/redistribution requires IEEE permission. See https://www.ieee.org/publications/rights/index.html for more information.